Comparative Analysis of Temperature Field and Stress Field of TC4 Titanium Alloy Joint Between CMT and MIG Welding

Rui ZHANG, Xiaoyan GU, Xiaopeng GU, Yu MENG, Lijuan ZHU

Key Laboratory of Automobile Materials, Ministry of Education, College of Materials Science and Engineering, Jilin University, Changchun, 130022, China, E-mail: ljzhu@jlu.edu.cn

1. Introduction

Cold metal transfer (CMT) technology is a new and revolutionary protective welding technology for gas metal arc welding. The CMT welding technology is different from the traditional MIG welding in droplet transfer mode. In the welding process, the droplet metal transition to the molten pool and the wire feeding process are combined to realize the short-circuiting transition at a very low current. This droplet transfer mode makes CMT welding have the advantages of small heat input, less splash and small post-weld stress and deformation [1 – 4]. Titanium alloy has excellent heat resistance and corrosion resistance, which is widely used in the aviation field. TC4 titanium alloy is a typical martensite α+β titanium alloy with excellent heat resistance, formability, weldability and corrosion resistance [5]. Due to the low Young's modulus of titanium alloy (about 110 GPa), the traditional TIG/MIG welding method has high heat input, which will lead to the difficulty of welding deformation and residual stress control of titanium alloy. Compared with MIG welding, CMT welding is a key technology to achieve high-precision and high-quality welding of titanium alloy with smaller heat input and lower residual stress [6]. The simulation of the CMT heat source is of great significance for process optimization and parameter analysis. Rna B et al. use parametric analysis to study the effect of plate thickness on welding deformation and residual stress of CMT lap joint of 1180 MPa steel. Finite element simulation of CMT composite pulse welding (CMT+P) narrow gap welding joint can also accurately predict the softening zone of aluminum alloy substrate [8]. A heat source model has been proposed by Azar et al. to simulate the effects of periodic arcs and metal deposition in CMT welding [9]. An improved model has been proposed by Zapico for automatic CMT welding based on the volume heat flux distribution of double ellipsoids over time [10]. However, there was no systematic comparative study on the temperature change and stress distribution of CMT and MIG welding joints from the perspective of numerical simulation. In the current study, based on the finite element theory, ANSYS finite element analysis software and APDL secondary development language were used to establish a CMT welding model based on the volume heat flow distribution of double ellipsoids loaded with time interval. The temperature field and stress field of CMT welding were studied and compared with that of MIG welding.

2. Numerical simulation modeling of temperature field in CMT molten pool

2.1. CMT welding heat source model

Since the heating effect of arc in the penetration direction should be considered in the CMT welding, the heat flow along the thickness direction has a great influence, which will produce a large weld depth-width ratio [11]. Therefore, the double ellipsoid heat source model is used to simulate the CMT heat source and the heat source model based on the double ellipsoid power density distribution is established. Eqs. (1) and (2) give expressions for the front and rear section volumetric heat fluxes according to this representation, respectively.

$$q_f(x, y, z) =$$
$$= \frac{6\sqrt{3}(f_f Q)}{a_h b_f c_h \pi \sqrt{\pi}} exp\left(-\frac{3x^2}{a_h^2} - \frac{3(y - vt)^2}{b_f^2} - \frac{3z^2}{c_h^2}\right), \quad (1)$$

$$q_r(x, y, z) =$$
$$= \frac{6\sqrt{3}(f_r Q)}{a_h b_r c_h \pi \sqrt{\pi}} exp\left(-\frac{3x^2}{a_h^2} - \frac{3(y - vt)^2}{b_r^2} - \frac{3z^2}{c_h^2}\right), \quad (2)$$

where: a_h, b_f, b_r and c_h are parameters relating to the heat source dimensions, mm; Q is the heat input, W, $Q = \eta UI$; η is the heat efficiency; U is the welding voltage, V; I is the welding current, A; v is the welding speed, mm/s; t is time, s; f_f and f_r are the distribution parameters of front and rear energy, $f_f + f_r = 2$.
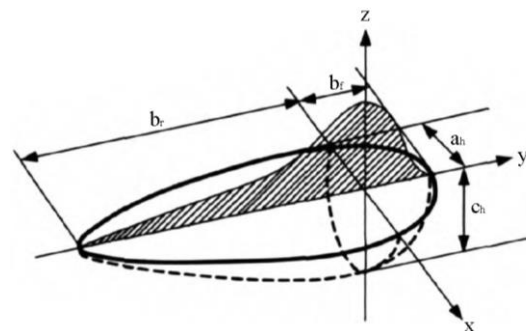
Fig. 1 Double ellipsoid heat source

As shown in Fig. 1, it is a double ellipsoidal heat source model, where the heat source is y axial symmetry and moves along the y-axis when loaded. In the welding process, the physical properties of the weldment will change when temperature increases. Since the heat source is constantly moving, the melting area of the weldment will experience rapid heating and rapid cooling. And the temperature field

is changing at all times. Therefore, the welding thermal process can be considered as a transient heat conduction problem with high nonlinearity [12]. The differential equation of nonlinear transient heat conduction is shown as follows:

$$\rho c \frac{\partial T}{\partial t} = \frac{\partial}{\partial x}\lambda\left(\frac{\partial T}{\partial x}\right) + \frac{\partial}{\partial y}\lambda\left(\frac{\partial T}{\partial y}\right) + \frac{\partial}{\partial z}\lambda\left(\frac{\partial T}{\partial z}\right) + Q(x,y,z,t),$$

where: $Q(x, y, z, t)$ is the intensity of the internal heat source; c is the specific heat capacity of the material; ρ is material density; λ is the thermal conductivity; t is the temperature field distribution function; T is the heat conduction time.

2.2. Establishment of finite element model

TC4 titanium alloy with a thickness of 2 mm was welded by CMT welding technology. Besides, the 1.2 mm TC4 welding wire with the same chemical composition as the base metal was selected. The size of the base metal was 75 mm × 50 mm × 2 mm, using pure argon as protective gas, and the butt joint was adopted. Before welding, the specimens were mechanically and chemically cleaned to remove oil pollution. As shown in Table 1, the thermal-physical properties of TC4 titanium alloy were obtained using JMatPro software.

The solid model and finite element model of the welding joint were shown in Fig. 2, a – c. The melting width was set as 4 mm and the reinforcement was taken as 1.5 mm. Due to the large temperature gradient at the weld seam, more accurate results were needed and the grid needed to be divided more accurately. The temperature gradient away from the weld was small, so the mesh needed to be coarser in order to reduce the amount of calculation. The gradual transition method was adopted to divide the grid. And the ratio factor of the maximum and minimum size of the grid was three. The solid model was discretized into 36966 nodes and 29200 elements.

Table 1

Thermal-physical properties of TC4

Temperature T, ℃	Young's modulus E, GPa	Possion's ratio ν	Density ρ, kg/m³	Specific-heat capacity C, J/(kg·K)	Thermal conductivity λ, W/(m·K)	Thermal expansion Coefficient α, 10^{-6}/℃
20	116	0.32	4450	611	6.82	9.1
100	112	0.32	4440	624	7.43	9.1
200	107	0.33	4430	653	8.74	9.2
400	96	0.33	4400	691	10.28	9.5
600	85	0.34	4370	713	13.72	10
800	75	0.35	4330	735	15.84	11
1000	70	0.38	4320	754	18.29	11
1200	63	0.39	4290	771	21.66	11
1400	55	0.40	4250	787	24.52	11
1600	47	0.41	4200	802	25.80	11
1660	45	0.41	4180	806	22	11
1800	0.12	0.50	4000	806	20	11
2000	0.12	0.50	3930	980	21	11
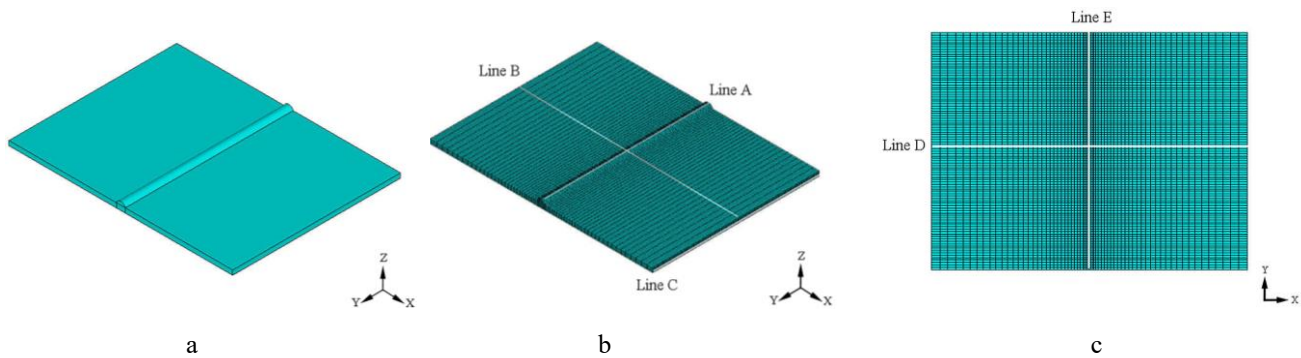
Fig. 2 Solid model and finite element model of welding joint

2.3 Processing of CMT welding heat source model

The CMT welding method is quite different from conventional MIG welding. In the normal CMT process, a CMT period can be divided into the arcing phase and short-circuiting phase. In the process of short-circuiting transition of CMT welding, the current and voltage of the power supply will be reduced to a very low level, where the heat input can be approximately considered as zero. At this time, it can be approximately considered that the heat input is zero. After the droplet transition is completed, the current is restored to the level of arcing stage. Therefore, it can be considered that the heat input in the CMT welding process is cyclical, which is characterized by zero heat input in the short-circuiting phase and normal heat input in the arcing phase in each droplet transition period.

In the calculation, t was adopted as a time cycle of droplet transition. When short-circuiting transition occurred in MIG welding, short circuit occurred between droplet and molten pool, accompanied by large current, resulting in large heat input. In the droplet transfer process of CMT welding, the wire was retracted to stimulate the detachment of droplet. The current was very small and the heat input was almost zero. To meet the real characteristics of CMT welding, periodic heat source loading was adopted and there existed a cooling period in each time cycle, which the heat

input could be considered as zero. Bi et al. carried out a large number of simulations and experimental data comparisons for this feature. It was proved that the cooling period of 0.3 t

would obtain more accurate results in each schedule t [13]. In this paper, 0.3 t was also used as a cooling period of droplet transition period.
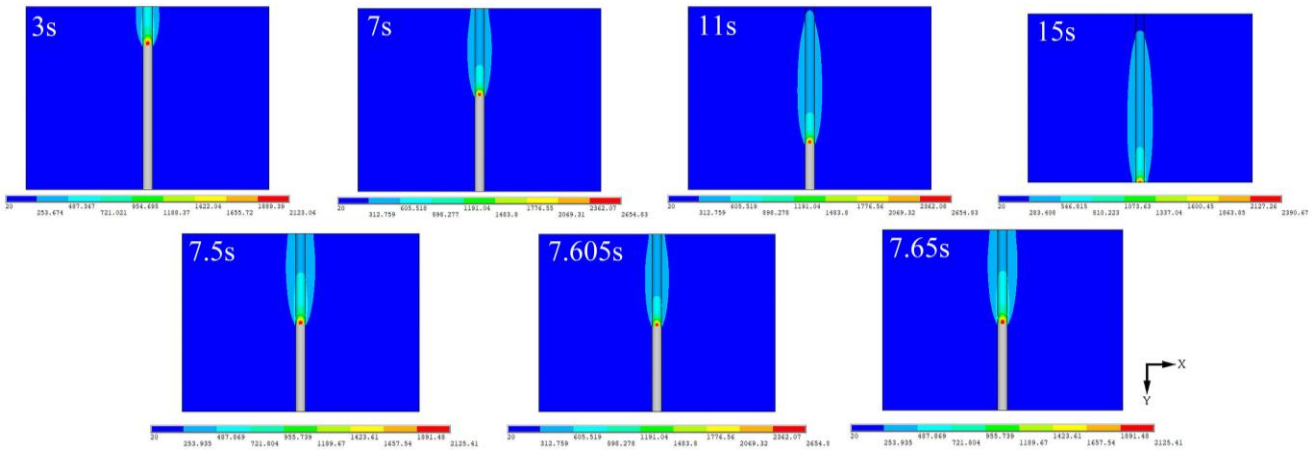
Fig. 3 Transient temperature field distribution of CMT welding
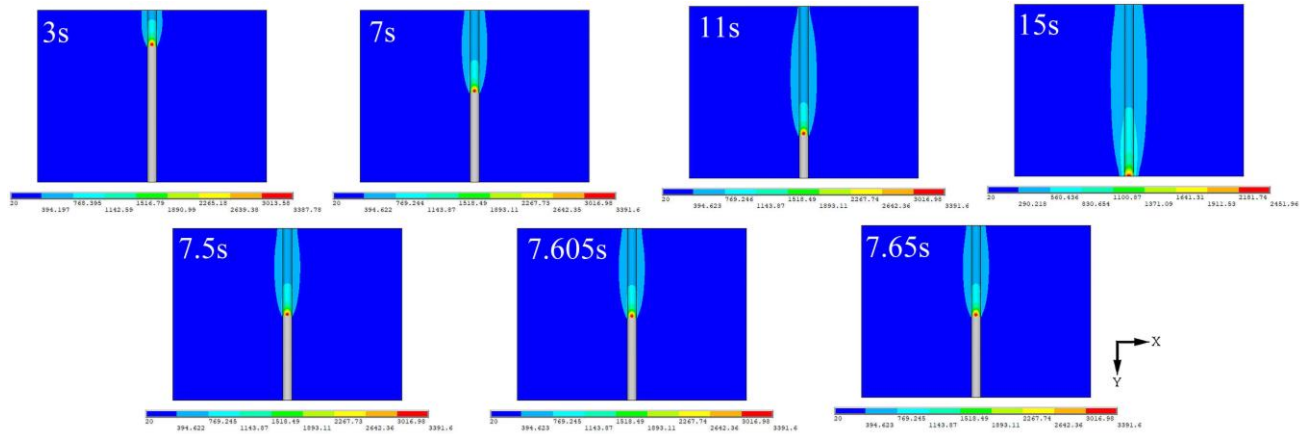
Fig. 4 Transient temperature field distribution of MIG welding

3. Comparative analysis of numerical simulation of molten pool temperature field between CMT and MIG welding

The welding parameters were as follows: welding voltage at 15.3 V, welding current at 114 A, wire feeding speed at 7 m/min, welding speed at 5 mm/s. When analyzing and calculating the temperature field of CMT welding and MIG welding, the same welding parameters were used. Different loading modes were used. The heat source of MIG welding was continuously loaded, while the heat source loading of CMT welding had a cooling period.

3.1. Numerical simulation of temperature field in CMT molten pool

According to the established three-dimensional transient heat transfer model, the temperature field of the CMT molten pool was calculated. Fig. 3 showed the temperature distribution of welding joint at different time (i.e. $t = 3$ s, 7 s, 11 s, 15 s, 7.5 s, 7.605 s and 7.65 s) when the heat source moved along line A (Fig. 2). Because the base metal and welding wire belonged to the same chemical composition and high-temperature properties, the temperature field cloud was symmetrical distribution. As shown in Fig. 3, the heat input increased gradually in the arcing stage and the temperature was in the rising stage. When the time changed

from 7 s to 11 s, the arc burned stably. The maximum temperature of the welding process was maintained at around 2655°C. Besides, the temperature decreased at the end of welding. Fig. 3 showed the temperature diagram of the CMT molten pool in a time cycle when the time changed from 7.5 s to 7.65 s. When the time was 7.5 s, the CMT heat source was in the stage of stopping loading. And the maximum temperature of the molten pool decreased. The CMT heat source was loaded when the time was 7.605 s, so the maximum temperature of the molten pool increased. In addition, the CMT heat source was stopped loading and the temperature of the molten pool decreased when the time was 7.65 s. Hence, the maximum temperature of the CMT heat
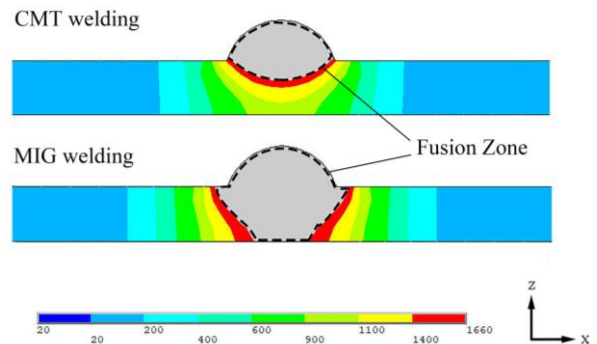
Fig. 5 Temperature distribution cloud diagram of cross-section of the CMT and MIG welding joint

source was fluctuating resulted from the loading of the thermal source with time interval.

3.2. Numerical simulation comparison of temperature field in molten pool between CMT and MIG welding

Fig. 4 showed the transient temperature distribution of MIG welding joint at different time (i.e. t = 3 s, 7 s, 11 s, 15 s, 7.5 s, 7.605 s and 7.65 s). It could be seen that the temperature change trend of MIG welding was the same as that of CMT welding. The maximum temperature of the welding joint was 3391.6°C when the time changed from 7 s to 11 s, which was much higher than that of CMT welding. It showed that the heat input of MIG welding was higher than that of CMT welding. Hence, the maximum temperature of the molten pool was higher. Fig. 4 showed the temperature distribution of MIG welding when the time changed from 7.5 s to 7.65 s. Compared with the fluctuant maximum temperature of the CMT molten pool, the maximum temperature of the MIG molten pool was unchanged due to continuous loading of the thermal source.

Fig. 5 showed the temperature distribution cloud diagram of cross-section of the CMT and MIG welding joint when the time was 7.5 s. Since the melting point of TC4 titanium alloy was 1660°C, the dotted line area with a temperature higher than 1660°C in the figure was the molten pool of the welding joint. It could be seen that the CMT welding joint was not penetrated. But the MIG welding joint was penetrated. The welding parameters of CMT welding and MIG welding were the same, the only difference was the loading method of the heat source. Compared with CMT welding, the molten pool of MIG welding was larger. At the same time, the melting width and penetration also increased. The reason was that the heat input increased with the continuous heat source loading of MIG welding. Besides, the heat was continuously transferred to the surrounding of the welding joint. It hindered the continuous transfer of heat to the sur-rounding when heat source was loaded intermittently, so the melting penetration and width were both smaller than that of MIG welding.

3.3. Thermal cycle curve of CMT welding

Fig. 6, a showed the CMT thermal cycle curves along line A (Fig. 2). It could be seen that the temperature gradually increased with the loading of the heat source. Since the welding speed was 5 mm/s, when the moving time of heat source was 3.75 s, 7.5 s and 11.25 s, the temperature reached the maximum 2654°C at the corresponding time. With the heat source loaded intermittently, the thermal cycle curve increased gradually in the form of fluctuation. The temperature decreased smoothly during cooling.

3.4. Comparison of thermal cycle curves between CMT and MIG welding

Fig. 6, b showed the MIG thermal cycle curves along line A (Fig. 2). Similar to the CMT thermal cycle curve, the temperature increased rapidly with the loading of the heat source and then gradually decreased. The difference was that the thermal cycle curve of the MIG welding did not fluctuate when the heat source was loaded, showing a smooth rise. And the maximum temperature of MIG welding was 3390°C, which was higher than that of the CMT

thermal cycle curve.

a

b
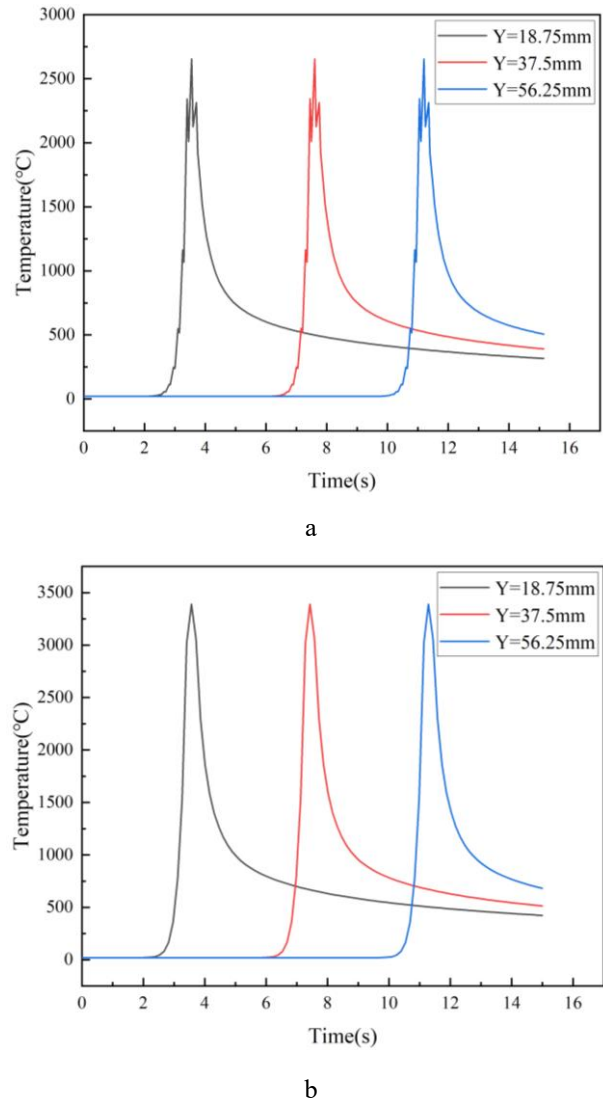
Fig. 6 Thermal cycle curve along line A: a - CMT welding; b - MIG welding

4. Simulation and comparative analysis of CMT and MIG residual stress

In the welding process, stress is caused by uneven distribution of temperature field. Therefore, when analyzing the stress field in the welding process, the temperature field results must be considered. The thermal-stress coupling analysis method is usually used to analyze the welding stress field.

In the current study, the sequential coupling method was used to calculate the stress field of TC4 titanium alloy joint. As shown in Fig. 7, three-point constraint was used to restrict three corners of the weld to prevent rigid displacement.

4.1. CMT welding residual stress simulation

The stress distributions of CMT welding after 515 seconds were given in Fig. 8. It could be seen that the stress distribution was asymmetrical and uniform, which was mainly caused by the same thermal-physical properties of base metal materials on both sides. The stress was relatively

low at the beginning and end of weld. And there was stress concentration at the weld, especially in the longitudinal stress distribution.

Fig. 9 showed the stress distribution curve of the upper and lower surface along line B and line D (Fig. 2). It could be seen from the diagram that the residual stress was mainly concentrated in the weld and heat-affected zone (HAZ). The curves of stress distribution trend in the residual stress simulation of TC4 titanium alloy were also obtained by ANN et al. [14]. The maximum von Mises stress on the upper surface was 501 MPa, which was about 160 MPa higher than that on the lower surface. The maximum longitudinal residual stress on the upper surface was 443 MPa, which was located in the center of the weld. The maxi-mum transverse residual stress was 98 MPa, located in the HAZ. The maximum normal residual stress was -118 MPa, located in the weld center. The transverse residual stress of the lower surface was mainly tensile and the maximum tensile stress was about 340 MPa, which was located in the center of the weld. Longitudinal tensile stress was about 86 MPa, concentrated in the weld zone. And normal compressive stress was about 46 MPa. It was found that stress concentration of

longitudinal stress and there existed normal stress in the weld zone. In addition, it was found that residual stress was sensitive to the weld distance. With the increase of the distance, the stress decreased greatly. The residual stress of the base metal outside the HAZ has decreased to below 100 MPa.

Fig. 7 Three-point constraint

a

b

c

d
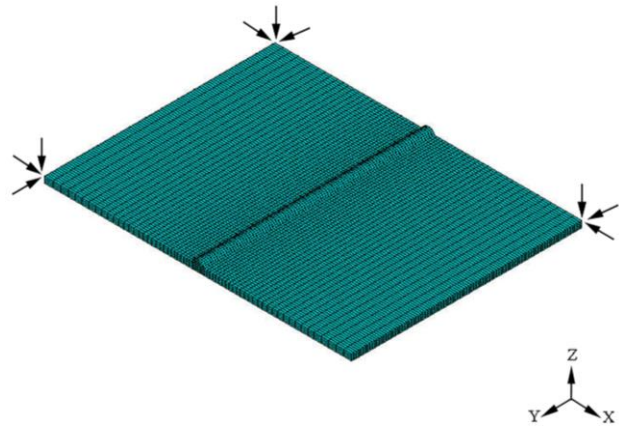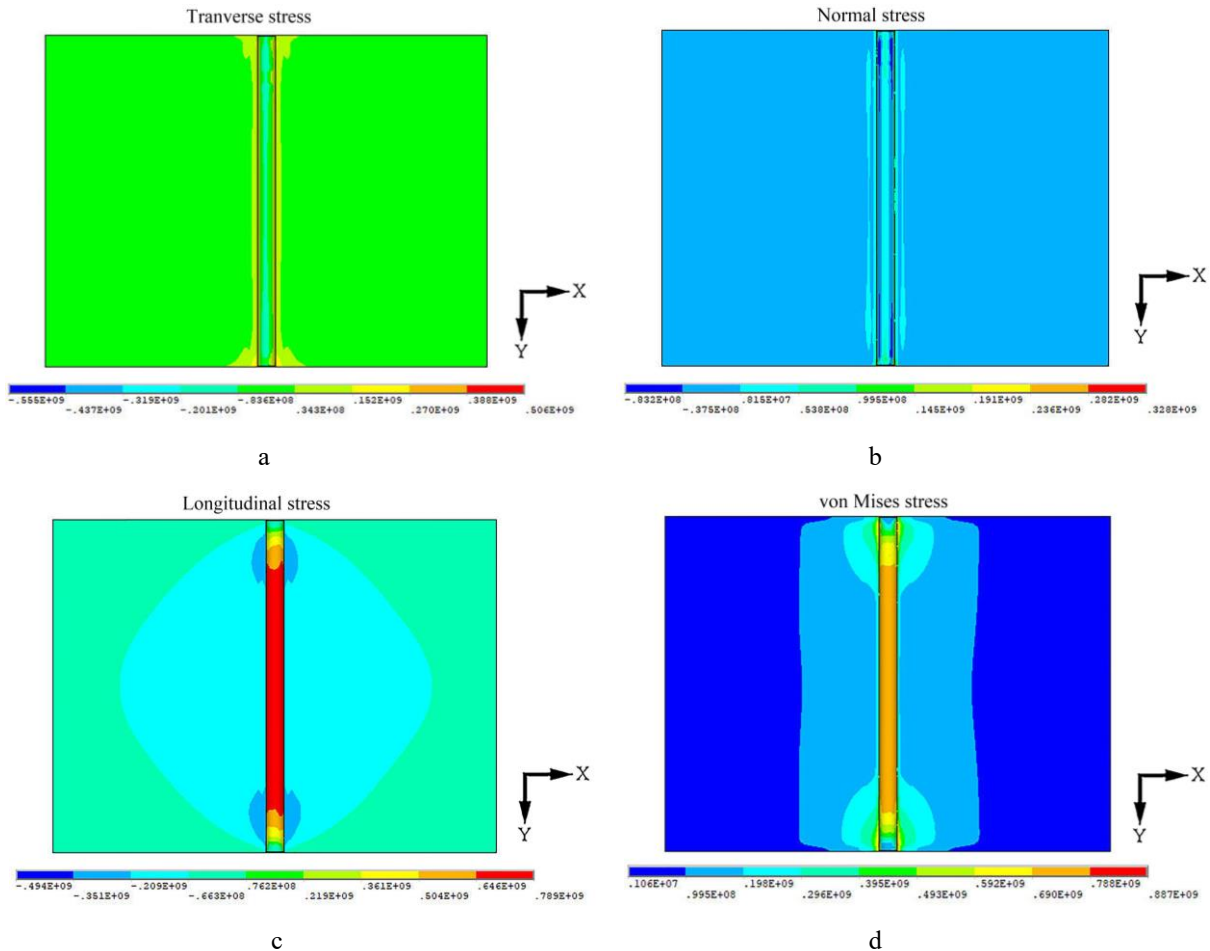
Fig. 8 Stress distribution diagram of CMT welding

Fig. 10 was the stress distribution curve of the upper and lower surface along line A and line E at the weld centerline (Fig. 2). It could be seen that the von Mises stress, longitudinal stress and transverse stress of the upper surface at the weld centerline were tensile. The maximum values were 746 MPa, 708 MPa and 180 MPa, respectively. Normal stress was compressive and the maximum value was

108 MPa. The von Mises stress of the lower surface at the weld centerline was tensile and the value was about 360 MPa. Transverse compressive stress was applied at the welding head and tail positions, and the maximum value was about 182 MPa. Normal stress was compressive stress and the maximum value was 59 MPa. Under the action of quasi-steady temperature field and constraint stress, the
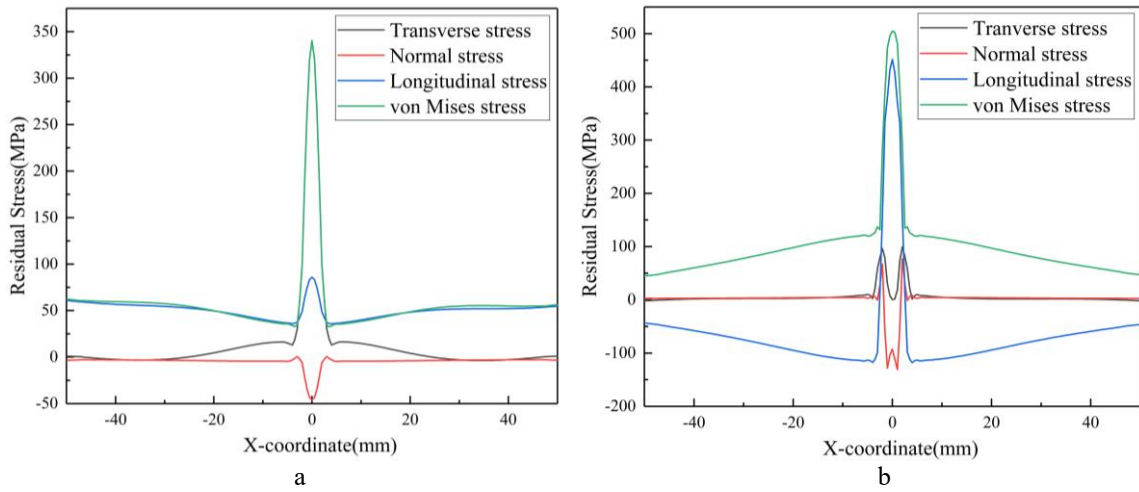
Fig. 9 Stress distribution curve of CMT welding: a - the upper surface along line B; b - the lower surface along line D
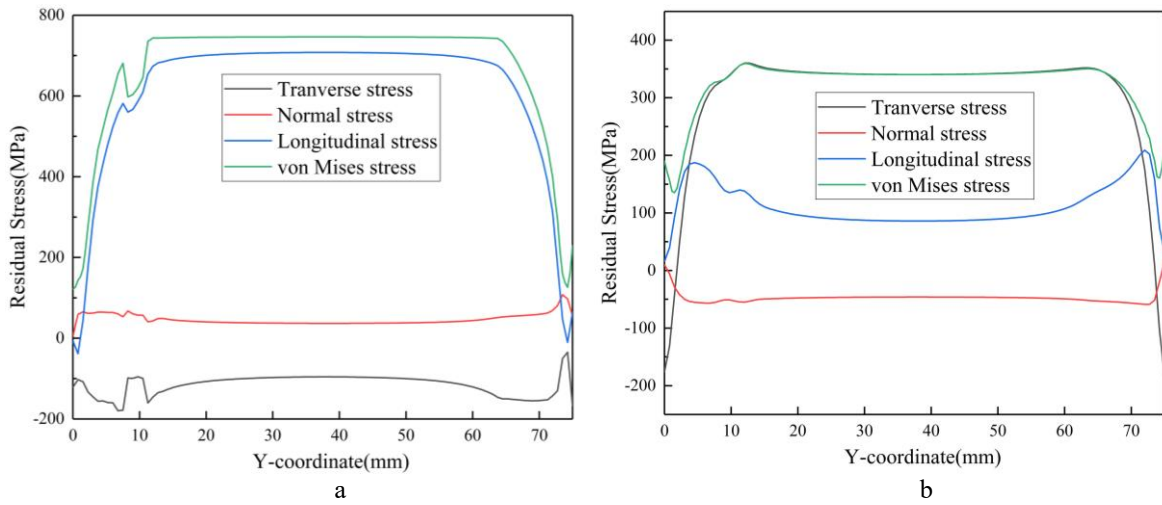
Fig. 10 Stress distribution curve of CMT welding: a - the upper surface along line A; b - the lower surface along line E
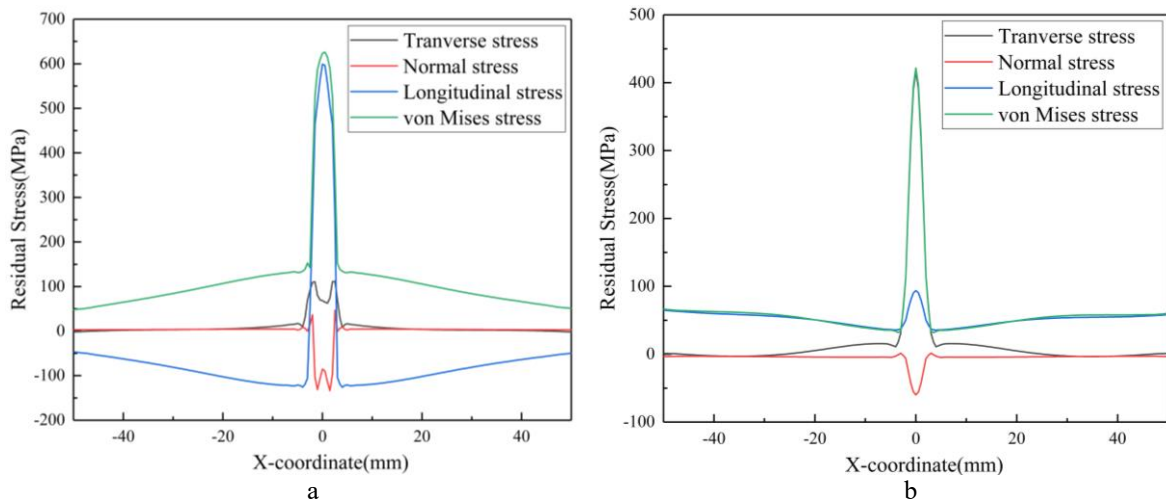
Fig. 11 Stress distribution curve of MIG welding: a - the upper surface along line B, b - the lower surface along line D

transverse and longitudinal residual stress of the upper surface weld center were stable at -100 MPa and 700 MPa except for the start and the end of weld. The transverse and longitudinal residual stress on the lower surface were stable at 350 MPa and 100 MPa. Contrary to the upper surface, the transverse stress at the center of the lower surface weld was mainly tensile due to the effect of weld cooling shrinkage.

4.2. Comparison of residual stress between CMT and MIG welding

Fig. 11 showed the stress distribution curve of the upper and lower surface of the MIG welding along line B and line D (Fig. 2). It could be seen from the diagram that the residual stress distribution trend of MIG welding was roughly the same as that of CMT welding, which was concentrated in the weld and HAZ. The maximum von Mises

stress on the upper surface of MIG welding was 626 MPa and the maximum von Mises stress on the lower surface is 422 MPa, which was greater than the residual stress value of CMT welding.

5. Comparative analysis of deformation after CMT and MIG welding

5.1. Comparison of angular deformation results between CMT and MIG welding

Fig. 12 showed the stress distribution of defor-

mation after CMT and MIG welding. Since the three-point constraint was adopted to prevent the rigid movement of the sample, it could be seen from the diagram that the stress distribution of welding joint was saddle-type. And the deformation value at both ends of the weld was small. The maximum deformation occurred in the weld of the middle part with the relatively free specimen. The highest temperature of the weld was in the middle part of the specimen during the cooling stage, so the shrinkage after welding was larger and the deformation value was the largest. Fig. 13, a was the angular deformation curve of CMT and MIG weld seams
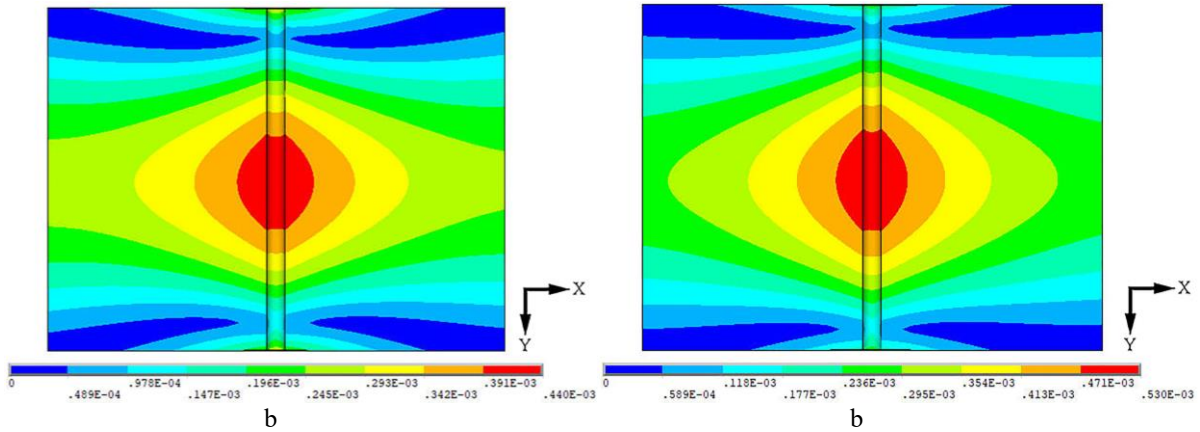
Fig. 12 Stress distributions of welding deformation: a - CMT welding; b - MIG welding
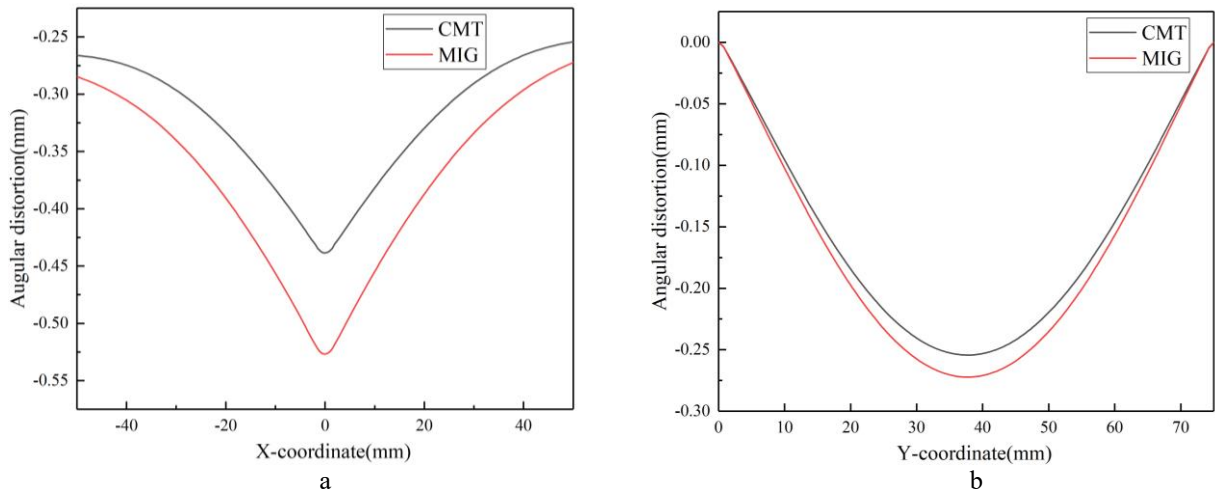
Fig. 13 Angular deformation curve: a - along line B; b - along line C
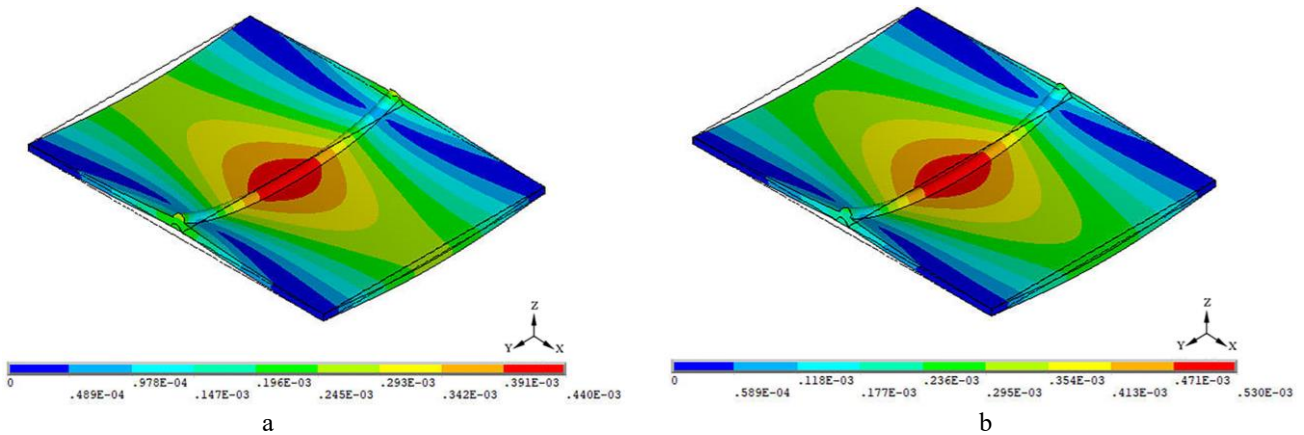
Fig. 14 Welding deformation diagram with ten times magnification: a - CMT welding; b - MIG welding

along line B (Fig. 2). It could be observed that the angular deformation along the x direction increased first and then decreased. And the displacement in the middle of the weld was the largest. The maximum angular deformation of CMT welding was 0.44 mm, while that of MIG welding was 0.53 mm. It was concluded that the larger shrinkage caused by cooling after welding was due to the larger heat input in MIG welding. Therefore, the deformation of MIG welding after welding was larger.

Fig. 14 showed the deformation diagram of CMT welding and MIG welding amplifying ten times. It could be seen from the diagram that the deformation of the downward recess occurred in the direction of the specimen. As shown in Fig. 13, b, the displacement curve in the y direction was extracted along line C (Fig. 2). It could be seen that the amount of deformation in the z direction was increased first and then decreased. Therefore, the maximum deformation occurred at the center of the weld. The maximum deformation of MIG welding was 0.27 mm, while the CMT was 0.25 mm. Therefore, the deformation of CMT welding was less than MIG welding.

5. Conclusions

With the model established in this paper, the temperature field that can show the characteristics of CMT welding is obtained. In addition, the comparison of temperature field and stress field between CMT and MIG welding is studied. The main conclusions can be summarized as follows:

1. When the heat source is loaded, the welding temperature of the CMT in the weld center is fluctuating and rising. And the maximum temperature of the CMT welding is 2654°C, the maximum temperature of MIG welding is 3390°C, which is higher than the maximum temperature of the CMT thermal cycle curve.

2. The residual stress distribution of the weld seam of the MIG welding is the same as that of the CMT welding, which is concentrated on the weld and HAZ. The maximum von Mises stress on the upper surface of the MIG welding is 626 MPa. And the maximum von Mises stress on the lower surface is 422 MPa, which is greater than the residual stress value of CMT welding.

3. Due to cooling shrinkage and other factors, welding deformation mainly occurs in the weld zone. The maximum angular deformation of CMT welding is 0.44 mm and the maximum angular deformation of MIG welding is 0.53 mm, which is greater than the welding angle of CMT welding.

References

1. **Pickin, C. G.; Williams, S. W.; Lunt, M.** 2011. Characterisation of the cold metal transfer (CMT) process and its application for low dilution cladding, Journal of Materials Processing Tech. 211(3): 496-502.
   http://dx.doi.org/10.1016/j.jmatprotec.2010.11.005.
2. **Wu, K. Y.; He, Z. W.; Dong, Z. L.,** et al. 2016. Numerical simulation of the temperature field of cold metal transfer welding pool, Mechanika 22(4): 285-290.
   http://dx.doi.org/10.5755/j01.mech.22.4.16163.
3. **Selvi, S.; Vishvaksenan, A.; Rajasekar, E.** 2018. Cold metal transfer (CMT) technology - An overview, Defence Technology 14(1): 17.
   http://dx.doi.org/10.3969/j.issn.2214-9147.2018.01.004.
4. **Cai, M.; Wu, C.; Gao, X.** 2018. The influence of arc length correction on welding in CMT welding, Iop Conference 170(4).
   http://dx.doi.org/10.1088/1755-1315/170/4/042106.
5. **Liu, W. Y.; Lin, Y. H.; Chen, Y. H.,** et al. 2017. Effect of different heat treatments on microstructure and mechanical properties of Ti6Al4V titanium alloy, Rare Metal Materials & Engineering 46(3): 634−639.
   https://doi.org/10.1016/S1875-5372(17)30109-1.
6. **Yuvaraj, N.; Vp, V.; Koli, Y.** 2020. Investigations on weld bead geometry and microstructure in CMT, MIG pulse synergic and MIG welding of AA6061-T6, Materials Research Express 6(12).
   https://doi.org/10.1088/2053-1591/ab61b6.
7. **Nishimura, R.; Ma, N.; Liu, Y.; Li, W.; Yasuki, T.** 2021. Measurement and analysis of welding deformation and residual stress in CMT welded lap joints of 1180MPa steel sheets, ScienceDirect 72: 515-528
   https://doi.org/10.1016/j.jmapro.2021.10.050.
8. **Shu, F.; Lü, Y.; Liu, Y.,** et al. 2014. FEM modeling of softened base metal in narrow-gap joint by CMT+P MIX welding procedure, Transactions of Nonferrous Metals Society of China 24(6): 1830–1835.
   https://doi.org/10.1016/S1003-6326(14)63260-X.
9. **Azar, A. S.** 2015. A heat source model for cold metal transfer (CMT) welding, Journal of Thermal Analysis and Calorimetry 122(2): 741-746.
   https://doi.org/10.1007/s10973-015-4809-4.
10. **Zapico, E. P.; Lutey, A.H.A.; Ascari, A.** et al. 2017. An improved model for cold metal transfer welding of aluminium alloys, Journal of Thermal Analysis & Calorimetry 131: 3003–3009.
    https://doi.org/10.1007/s10973-017-6800-8.
11. **Goldak, J.; Chakravarti, A.; Bibby, M.** 1984. A new finite element model for welding heat sources, Metall Trans B 15(2): 299-305.
    https://doi.org/10.1007/BF02667333.
12. **Okano, S.; Tanaka, M.; Mochizuki, M.** 2013. Arc physics based heat source modelling for numerical simulation of weld residual stress and distortion, Science & Technology of Welding & Joining 16(3): 209-214.
    https://doi.org/10.1179/1362171810Y.0000000019.
13. **Bi, K. Q.** 2015. The research on numerical simulation of welding temperature field and processing parameters in CMT welding [D], Nanchang University.
14. **Ahn, J.; He, E.; Chen, L.,** et al. 2017. Prediction and measurement of residual stresses and distortions in fibre laser welded Ti-6Al-4V considering phase transformation, Materials & design 115: 441-457
    http://dx.doi.org/10.1016/j.matdes.2016.11.078.

R. Zhang, X. Y. Gu, X. P. Gu, Y. Meng, L. J. Zhu

COMPARATIVE ANALYSIS OF TEMPERATURE FIELD AND STRESS FIELD OF TC4 TITANIUM ALLOY JOINT BETWEEN CMT AND MIG WELDING

S u m m a r y

A model was used for the cold metal transfer (CMT) welding based on the volume heat flux distribution of double ellipsoids loaded with time intervals. The temperature

field and stress field of TC4 titanium alloy were numerically simulated by ANSYS software. The distribution laws of temperature, residual stress and post-weld deformation during CMT and MIG welding were studied and compared. It was found that the maximum temperature of the molten pool in CMT welding was fluctuating and rising during the loading process, while the temperature of the molten pool in MIG welding was rising smoothly and the maximum temperature was higher than that in CMT welding. The welding stress field was analyzed by thermal-stress coupling analysis. The stress distribution simulated based on the MIG welding heat source was similar to CMT welding, but the maximum von Mises stress was greater than that of CMT welding. Due to the cooling shrinkage, both of them would produce angular deformation after welding. And the maximum angular deformation simulated based on the MIG welding heat source was greater than that of CMT welding. It was proved by welding simulation that CMT welding could reduce welding heat input and residual stress and deformation after welding.